Available online at www.sciencedirect.com
SCIENCE DIRECT
Polymer 46 (2005) 5621–5629
polymer
www.elsevier.com/locate/polymer

Poly(ethylene 2,6-naphthalate)/layered silicate nanocomposites: fabrication, crystallization behavior and properties

Tzong-Ming Wu*, Chuh-Yi Liu

Department of Material Science and Engineering, National Chung Hsing University, 250 Kuo Kuang Road, Taichung 402, Taiwan, ROC

Received 17 September 2004; received in revised form 27 April 2005; accepted 29 April 2005
Available online 31 May 2005

Abstract

In this study, poly(ethylene 2,6-naphthalate) (PEN)/layered silicate nanocomposites (PLSNs) were successfully prepared by the intercalation of PEN polymer into organically-modified layered montmorillonite through the melt blending process. Both X-ray diffraction data and transmission electron microscopy images of PEN/layered silicate nanocomposites indicate most of the swellable silicate layers were exfoliated and randomly dispersed into the PEN matrix. Mechanical and barrier properties of the fabricated nanocomposites performed by dynamic mechanical analysis and permeability analysis show significant improvements in the storage modulus and water permeability when compared to neat PEN. Differential scanning calorimeter (DSC) was used to investigate the isothermal crystallization behavior and melting behavior of PLSNs. DSC isothermal results revealed that the crystal growth process of PEN and PLSNs are a three-dimensional spherulitic growth. The activation energy of PEN increases with increasing content of layered silicates. The result indicates that the addition of layered silicate into PEN reduces the transportation ability of polymer chains during crystallization processes.

Keywords: Poly(ethylene 2,6-naphthalate); Nanocomposite; Structural behavior

1. Introduction

Polymer layered silicate nanocomposites (PLSNs) have been the focus of academic and industrial attention in recent years because the final composites often exhibit a desired enhancement of physical and/or chemical properties relative to the neat polymer matrix [1–5]. The synthesis of PLSNs is done by the intercalation of monomers or polymers into swellable layered silicate hosts. In most cases, the synthesis involves either intercalation of a suitable monomer and then exfoliating the layered host into their nanoscale elements by subsequent polymerization or melt-direct polymer intercalation by using a conventional polymer extrusion process [6–8]. The high aspect ratio layered silicate affects the mechanical, physical and thermal properties of the synthesizing polymer nanocomposites.

Poly(ethylene 2,6-naphthalate) (PEN) has received considerable attention due to its superior strength, low permeability to gases and excellent thermal stability [9,10], which is a possible candidate used in flexible substrate display. Crystallization studies of PEN including crystalline structure [11–13], crystallization kinetics [13], liquid-induced crystallization [14], structural change/formation during uniaxial [15–18] or biaxial drawing [15], flow-induced crystallization [19], and crystal morphology [20–23] have recently been reported and revealed a complex polymorphic behavior. The various crystalline structures differ with respect to the chain conformation and the chain packing within a unit cell. Two major crystalline forms, α and β form, were determined by Mencik [11] and Zachmann et al. [12] as triclinic unit cells with $a=6.51$ Å, $b=5.75$ Å, $c=13.2$ Å, $\alpha=81.33°$, $\beta=144°$, $\gamma=100°$ and $a=9.26$ Å, $b=15.59$ Å, $c=12.73$ Å, $\alpha=121.6°$, $\beta=95.57°$, $\gamma=122.52°$, respectively. Various effects on polymeric behavior of PEN are dependent on the crystallization condition such as crystallization temperatures and pre-melting temperatures [11–15]. Nevertheless, no further work appears and a deep understanding of the formation of both crystalline forms is still lacking.

It is well known that the physical and mechanical

* Corresponding author. Tel.: +886 4 22840500x806; fax: +886 4 22857017.
E-mail address: tmwu@dragon.nchu.edu.tw (T.-M. Wu).

0032-3861/$ - see front matter © 2005 Elsevier Ltd. All rights reserved.
doi:10.1016/j.polymer.2005.04.071

properties of crystalline polymers depend on the structure and the morphology of the polymer crystallites and on the degree of crystallization. It has been recently found that the crystallization behavior and crystalline morphology of polymer nanocomposites are strongly affected by the presence of the layered silicates, including of polyamide [24–26], polypropylene [27–29], poly(ε-caprolactone) [30,31] and syndiotactic polystyrene [32–34]. General effects included induced polymorphism [24–27,32–34], small and irregular crystallite [27], increased crystallization rate [31–33] and alteration of the crystal fraction [32]. The extent of these effects depends on process history and specific characteristics of the resin.

In this report, we have used organically-modified montmorillonite as the dispersed phase to prepare PEN/layered silicate nanocomposites by melt-direct intercalation of PEN into swellable layered hosts. Due to the presence of rigid naphthalene ring in its backbone, it was not thought that homogeneous dispersion of the silicate layers in PEN would be realized. Therefore, the montmorillonite has been modified by *n*-hexadecyl trimethyl-ammonium bromide (CTAB) cations and then polymerized by a mixture of styrene and methyl methacrylate monomer at a styrene/-methyl methacrylate ratio of 8/2 with potassium presulphate as a catalyst to provide the chemical similarity between polymer matrix and surface-modified clay, which may further improve their interaction. The PLSNs have been prepared through the direct insertion of PEN polymer chains from the melt into the surface-treated clay. A conceptual illustration of the preparation of PLSNs is shown in Fig. 1. X-ray diffraction data indicate most of the swellable silicate layers were exfoliated and randomly dispersed into the PEN matrix. To the best of our knowledge this is the first report of exfolicated silicate layers within a PEN matrix. The physical properties of prepared nanocomposites were measured by dynamic mechanical analysis (DMA) and permeability analysis. Since the final mechanical properties of PLSNs are directly related to the crystalline features and behaviors [35,36], it is necessary to characterize the microstructure of PLSNs during formation. In particular, the addition of small amount of nanoscale layered silicate into PEN affected their crystalline behaviors during sample formation. This work is focused on the isothermal melt-crystallization kinetics and melting behavior of PLSNs from DSC thermal analysis. The parameters of crystallization kinetics, such as the laternal-surface and fold-surface energy of isothermal crystallization as well as the activation energy of PEN and PLSNs can also be discussed.

2. Experimental

2.1. Preparation of PLSNs

The poly(ethylene 2,6-naphthalate) (PEN) with weight average molecular weight (M_w) of 60,000 was kindly supplied by Union Chemical Laboratory (Hsinchu, Taiwan). Natural sodium montmorillonite (MMT) with a cation exchange capacity (CEC) of 110 mequiv/100 g was used as the dispersed phase to reinforce the PEN. The surface of natural sodium MMT was modified by cationic exchange between Na^+ in MMT galleries and *n*-hexadecyl trimethyl-ammonium bromide (CTAB) cations in an aqueous solution at 60 °C for 2 h. The exchanged MMT was then polymerized with a mixture of styrene and methyl methacrylate monomer at a styrene/methyl methacrylate ratio of 8/2 with potassium presulphate (KPS) as a catalyst. The PLSNs were prepared by a melt-direct intercalation process using

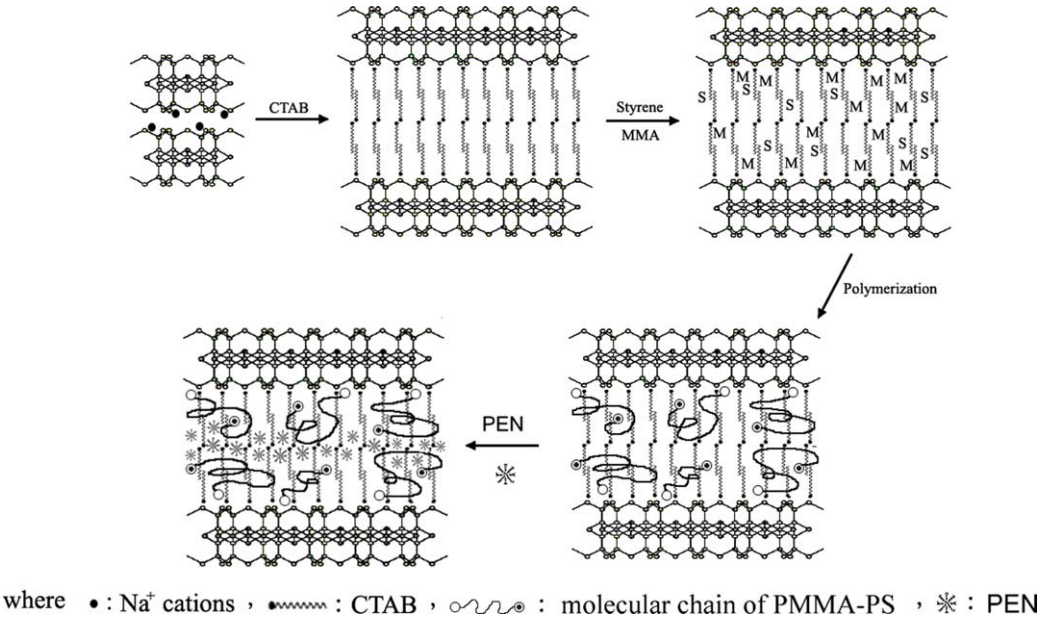

Fig. 1. Schematic representation of the preparation of PEN/organically-modified clay nanocomposites.

surface-treated MMT and PEN at 280 °C in a Haake mixer for 10 min.

Samples of pure PEN and PLSNs were sandwiched between two cover glasses and heated on a hot stage at pre-melting temperature (T_{max}) of 300 °C. The sample was pressed into a thin film with thickness in the range of 0.03 mm by tweezers, kept for 20 min to eliminate any thermal history and the memory of crystalline form in the melt and then cooled to the proposed crystallization temperatures (T_{cs}) in the range of 228–240 °C.

2.2. Characterization

X-ray $\theta/2\theta$ diffraction scans of these specimens were obtained using a 3 kW Rigaku III diffractometer equipped with Ni-filtered Cu K_α radiation in the reflection mode. Thermal analysis of the samples was preformed using a Perkin–Elmer PYRIS Diamond differential scanning calorimeter (DSC) calibrated using indium and all experiments were carried out under a nitrogen atmosphere. All specimens were in the range of 5–6 mg. For isothermal crystallization, the specimens were heated to $T_{max} = 300$ °C at a rate of 100 °C/min and held for 20 min to remove the residual crystals, then they were quickly cooled to the proposed crystallization temperatures (T_{cs}) in the range of 228–40 °C. Heat fusion versus time for isothermal crystallization (ΔH_c) was recorded. Therefore, the crystallization temperature (T_c), exothermic heat of crystallization (ΔH_c), crystalline melting temperature (T_m), and heat of fusion of polymer crystalline (ΔH_m) for the PEN and PLSNs are recorded. The specimens isothermally crystallized at the crystallization temperatures were heated to $T_{max} = 300$ °C at a rate of 10 °C/min.

Transmission electron microscopy was carried out with a JOEL transmission electron microscope using an acceleration voltage of 120 keV. Ultrathin section of the PEN/clay film with a thickness of approximate 50 nm was prepared with an ultramicrotome equipped with a diamond knife. Due to the high electron density difference between silicate and polymer matrix, staining of the samples was not necessary. Dynamic mechanical analysis (DMA) experiments were performed on a Perkin–Elmer instrument DMA 7e apparatus equipped with a film tension clamp. The instrument was programmed to measure E' (storage modulus) over the range of 30–170 °C at 2 °C/min heating rate and 1 Hz constant frequency. Calibrations for force, mass, position, and temperature were made in accordance with Perkin–Elmer procedures. The specimen films were cut with length-to-width ratios > 6 to guarantee uniform strain of the samples and the collected data were reproducible. Permeability measurements for water were performed on a 25-cm^2 active sample area at 100% relative humidity and 40 °C using a MOCON PERMATRAN-W 3/61 instrument. Water transmission was measured for the neat PEN and PLSNs with a nominal thickness of 100 μm.

3. Results and discussion

3.1. Morphology of PLSNs

Fig. 2 (curves (a) and (b)) shows X-ray diffraction data of neat layered montmorillonite and montmorillonite modified with a mixture of CTAB, ST and MMA. It is clear that the X-ray peaks shift to smaller angle for the organically modified montmorillonite. The interlayer distances of the silicates were obtained from the peak position (d_{001}-reflection) of WAXD traces. The d_{001}-reflection for the neat layered montmorillonite was found at a $2\theta \approx 7.12°$, which corresponds to an interlayer distance of 12.5 Å (Fig. 2, trace a). Surface modification by CTAB cations and PMMS/PS polymer chains afforded substantially increased interlayer distances of montmorillonite. The X-ray reflection of surface-modified clay (trace b in Fig. 2) was found at $2\theta \approx 2.40°$, corresponding to an interlayer distance of 36.8 Å. The X-ray diffraction curves of 1 and 3 wt% PLSNs are also shown in Fig. 2. Both X-ray diffraction scans of nanocomposites exhibited no d_{001}-reflection in the relevant region, thus indicating the presence of interlayer distances at least larger than 48 Å or no regular periodicity. These results also show that PEN can be well dispersed in the surface-treated layered montmorillonite, thus further increasing the interlayer distances of montmorillonite. Although X-ray is the simplest method to measure the interlayer distance of montmorillonite, TEM was also used to visually evaluate the degree of intercalation and the amount of aggregation of layered silicate clusters. Fig. 3 shows transmission electron microscopy micrographs of 3 wt% PLSN in which the gray areas represent the silicate layers in the PEN matrix (bright). From the TEM results, the layered silicate is well separated in the PEN matrix. Therefore, all those results demonstrated that most of PEN is exfoliated into the swellable silicate layers.

3.2. Physical properties of PLSNs

Fig. 4 shows the temperature dependence of the storage tensile modulus, G', of the neat PEN and PEN with different layered silicate loadings over the range of 30–170 °C. Each of the curves represents at least three different measurements providing a standard deviation $< \pm 20$ MPa. An apparent glass transition is revealed by a steep decrease of storage modulus followed by the initial glassy plateau in all of the samples. This temperature is not significantly affected by the incorporation of layered silicates. Over the entire temperature range, the storage modulus of the 3 wt% layered silicate content sample is higher than that of 1 wt% PLSN and neat PEN. Around room temperature the amounts of improvement in storage modulus for 1 and 3 wt% loadings are 25.7 and 51.3%, respectively, compared to neat PEN. On the other hand, at higher temperatures, above 140 °C, all the samples reach a plateau, which suggests a rubber-like structure composed of both crystalline

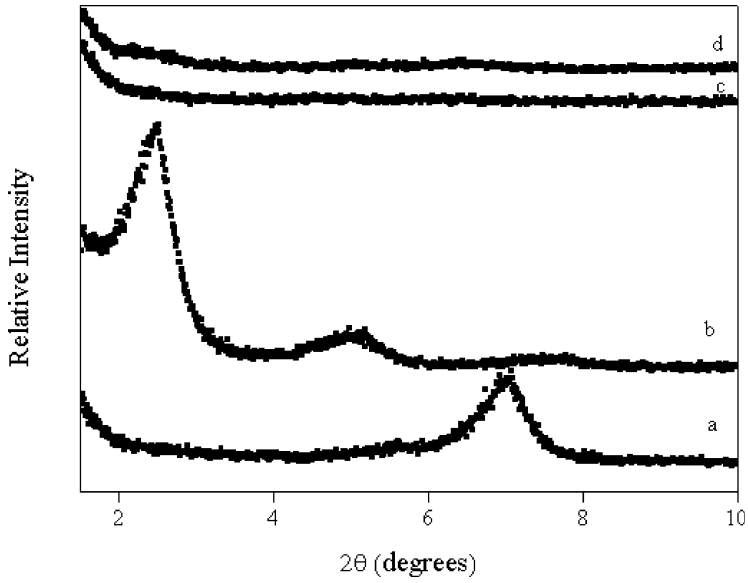

Fig. 2. X-ray diffraction scans of (a) neat layered montmorillonite, (b) surface modified montmorillonite, (c) 1 wt% PLSNs and (d) 3 wt% PLSNs.

and amorphous phases. In plateau regions above 140 °C, the enhancement in storage modulus of PLSNs compared to pure PEN is decreased to only 5–8%. This phenomenon is also observed in other polymer/clay systems in which, after a specific temperature, the effect of layered silicate on the storage modulus becomes less significant and the nanocomposite stiffness becomes matrix dependent [4,5]. At the temperature above 140 °C, it has almost reached the softening point of the PEN matrix which strongly reduce the elastic response of the fabricated materials.

Another important feature of the PLSNs is their excellent barrier properties. Water permeability of the neat PEN and PLSNs were measured and the results are 11.5, 4.5 and 3.3 gm/m^2 day for PEN, 1 and 3 wt% PLSNs. In the 1 wt% PLSNs, there is a large decrease in the water permeability, indicating a significantly improved water-barrier property of the PEN. The reduction of permeability arises from the longer diffusive path that the pentrants must travel in the presence of the layered silicates. The reduction of water permeability is further decreased with increasing the content of layered silicate to 3 wt%.

3.3. Crystallization behavior of PLSNs

The crystallization kinetics of PEN and PLSNs can be

Fig. 3. TEM micrographs of 3 wt% PLSNs. Silicate platelets are visible as grey areas.

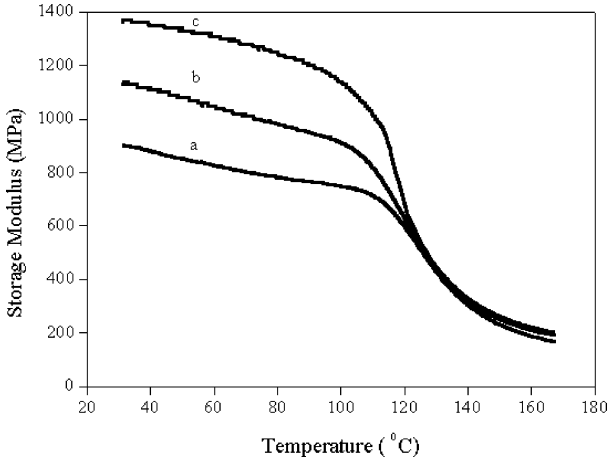

Fig. 4. Dynamic viscoelastic behavior of (a) neat PEN, (b) 1 wt % PLSNs and 3 wt % PLSNs.

analyzed by using classical Avrami equation [37,38] as given in Eq. (1)

$$1 - X_t = \exp(-kt^n) \tag{1}$$

where X_t is the development of crystallinity X_c at time t. The time ($t_{1/2}$), at which half crystallization occurs, can be assumed. The fraction of X_t is obtained from the area of the exothermic peak in DSC isothermal crystallization analysis at a crystallization time t divided by the total area under the exothermic peak.

$$X_t = \frac{\int_0^t \frac{dH}{dt} dt}{\int_0^\infty \frac{dH}{dt} dt} = \frac{\Delta H_t}{\Delta H_0} \tag{2}$$

where the numerator is the heat (ΔH_t) generated at time t and the denominator is the total heat (ΔH_0) generated up to the complete crystallization. In Eq. (1), the k value is the crystallization rate constant (min^{-1}) and n value is the Avrami exponent. Both k and n depend on the nucleation and growth mechanisms of spherulites. In order to convert conveniently with the operation, Eq. (1) can be transformed into

$$\ln[-\ln(1 - X_t)] = n \ln t + \ln k \tag{3}$$

Fig. 5 shows the plot of $\ln[-\ln(1-X_t)]$ versus $\ln t$ for PEN. The k and n values could be directly obtained using Eq. (3) from the intercept and slope of the best-fitting line. The crystallization behavior is usual to distinguish the linear stage, i.e. before the kinetic curve deviates markedly from the theoretical isotherms, as well as the primary crystallization from the non-linear stage for the secondary crystallization. The primary crystallization consists of the outward growth of lamellar stacks until impingement and the secondary crystallization, which may overlap the primary crystallization, is filling in the spherulites of interstices. Many results have been suggested that both primary and secondary crystallization were incorporated into Avrami theory [39]. In the present work, we focus only on primary crystallization. Several crystallization parameters $t_{1/2}$, k, and n of PEN and PLSNs are summarized in Table 1. The plots of $\ln[-\ln(1-X_t)]$ versus $\ln t$ for 1 and 3 wt% PLSNs show similar tendency and their crystallization parameters are also listed in Table 1. The isothermal crystallization rates of PEN and PLSNs conducted by $1/t_{1/2}$ decrease as T_c increases and increases with the increasing the content of layered silicate. These indicate that the additional content of layered silicate does affect the crystallization behaviors of the PEN. It is also found n values are dependent on the content of layered silicate and T_c.

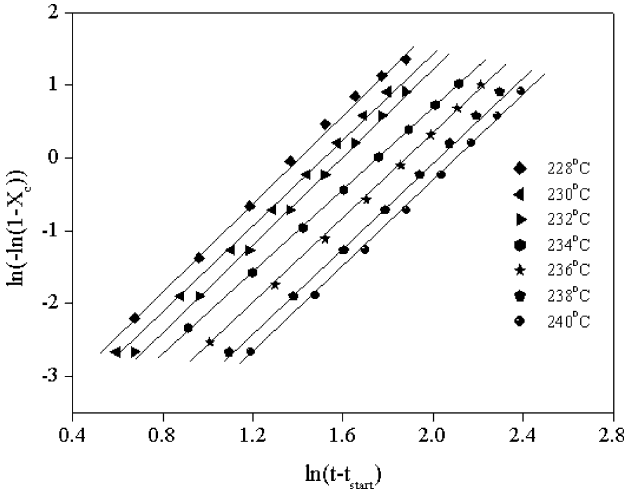

Fig. 5. Avrami plots of $\ln[-\ln(1-X_t)]$ versus $\ln t$ for PEN.

For PEN sample, the n values range around 2.8–3.0 as the increasing T_c. In general, a value of n close to 3 may represent an athermal nucleation process followed by a three-dimensional crystal growth. On the other hand, the value of $n \approx 2.0$–2.2 indicates that crystal growth may not occur in three dimensions at an equal rate and hence a low n value may be obtained. The non-integral n values we obtained might be due to the presence of crystalline branching and/or two stage crystal growth during the crystallization process and/or mixed growth and nucleation mechanism [40]. The n values of 1 wt% PLSNs are also in the range of 3.1, which are close to those of PEN. Addition of more layered silicate into PEN up to 3 wt%, the n values are in the range of 2.7–2.9 and are close to those of PEN and 1 wt% PLSNs. Therefore, these results indicate that the spherulitic formation of PEN and PLSNs are similar and the introduction of clay into the PEN remain the crystal growth process from a three-dimensional spherulitic growth. In addition, the values of the crystallization rate parameters k are apt to decrease with increasing T_c due to a gradual decrease in the degree of supercooling. At the same time, the values of k increase with increasing clay content, indicating a significant increase in the heterogeneous nucleation for PLSNs.

The crystallization rate parameter k can also be approximately described as follows:

$$\frac{1}{n}(\ln k) = \ln k_0 - \frac{\Delta E}{RT} \tag{4}$$

where k_0 is a temperature-independent pre-exponential factor; ΔE is a total activation energy, which consists of the transport activation energy ΔE^* and the nucleation activation energy ΔF (ΔE^* refers to the activation energy required to transport molecular segments across the phase boundary to the crystallization surface and ΔF is the free energy of formation of the critical size crystal nuclei at T_c); R is the universal gas constant. Arrhenius plots of $1/n$ ($\ln k$) against $1/T$ for PEN and PLSNs are shown in Fig. 6, and are approximately linear. The activation energy can be determined from the slope of plots and is strongly dependent on the content of layered silicate. The activation energy slightly increases with increasing the content of layered silicate. The result indicates that the addition of more

Table 1
Values of $t_{1/2}$, k, and n at various T_c for PEN and PLSNs

T_c (°C)	228	230	232	234	236	238	240
PEN							
$t_{1/2}$	3.57	4.04	4.36	5.16	5.87	6.66	7.35
k	0.014	0.011	0.009	0.0007	0.004	0.002	0.002
n	3.04	2.99	3.00	2.81	2.95	3.00	3.00
1 wt% PLSN							
$t_{1/2t}$	1.54	2.07	2.37	2.65	2.97	3.39	4.14
k	0.093	0.067	0.048	0.033	0.023	0.015	0.009
n	3.10	3.12	3.10	3.10	3.10	3.10	3.11
3 wt% PLSN							
$t_{1/2}$	1.09	1.31	1.42	1.61	1.81	2.41	2.81
k	0.422	0.330	0.224	0.155	0.113	0.050	0.033
n	2.92	2.82	2.79	2.95	2.74	2.91	2.86

layered silicate into the PEN matrix causes more heterogeneous nucleation, which is expected to obtain a lower ΔE. But the addition of more layered silicate induced more steric hindrance also reduces the transportation ability of polymer chains during crystallization processes (a higher ΔE), the ΔE of PLSNs increases as the content of layered silicate increases from 1 to 3 wt%. Detail activation energy of PEN and PLSNs are shown in Table 2.

Fig. 7 shows the DSC heating scans of PEN and 3 wt% PLSNs after completion of isothermal crystallization at various T_c and then are heated directly from T_c to T_{max} = 300 °C at a heating rate of 10 °C/min. It can be clearly seen that the DSC heating curves of these specimens contain only two endotherm behaviors. The first melting endotherm (referred as T_m(I)) associated with the fusion of crystals grown at T_c is corresponding to the thermodynamically most stable β crystalline form. The second melting endotherm (referred as T_m(II)) is attributed to the melting of crystallite that was formed by melting and recrystallization during the DSC heating scans. Recrystallization involving crystal perfection and crystal thickening could melt at higher temperatures, depending upon the degree of perfection achieved.

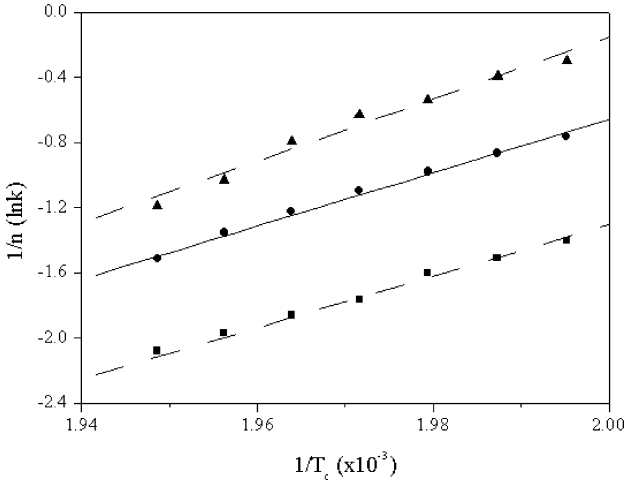

Fig. 6. Arrhenius plots of $1/n$ (ln k) versus $1/T$ for PEN and PLSNs.

The equilibrium melting temperature T_m^0 of the PEN and PLSNs can be determined by the plot of T_m versus T_c according to Hoffman and Week's equation [41,42]:

$$T_m = T_m^0\left(1 - \frac{1}{\gamma}\right) + \frac{T_c}{\gamma} \quad (5)$$

where γ is a factor depending on the final laminar thickness.

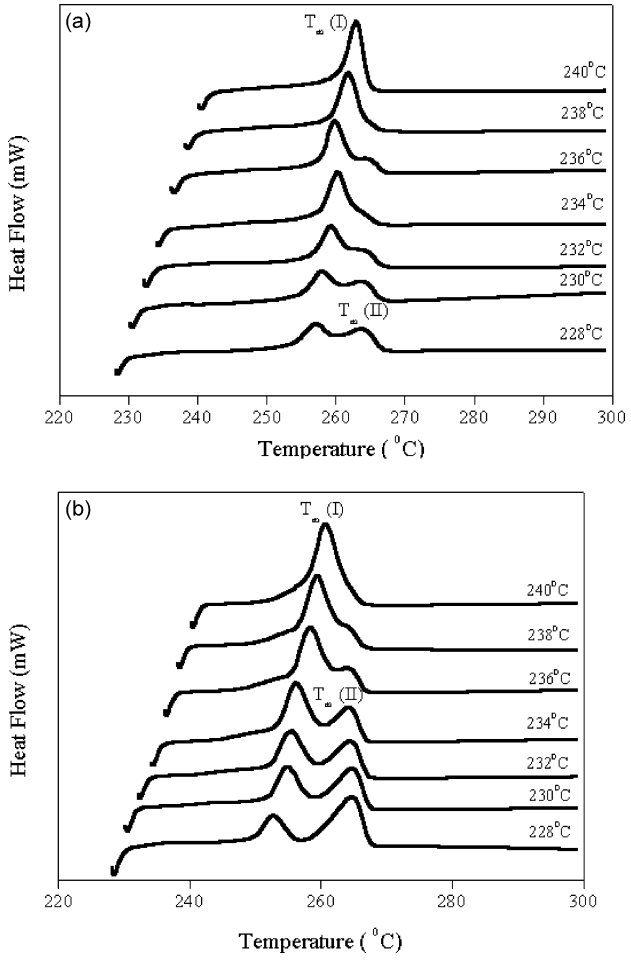

Fig. 7. DSC thermograms of (a) PEN and (b) 3 wt% PLSNs cooled from T_{max} = 300 °C at various T_cs.

Table 2
Values of E_a, T_m^0, K_g, G_0 and$\sigma\sigma_e$ at various T_c for PEN and PLSNs

	PEN	1 wt% PLSN	3 wt% PLSN
E_a (kJ/mol)	131.09	136.15	158.28
T_m^0 (K)	555.23	565.01	564.07
K_g (K^2)	1.30×10^5	2.10×10^5	2.09×10^5
$\sigma\sigma_e$ (J^2/m^4)	9.15×10^{-4}	14.68×10^{-4}	14.64×10^{-4}
σ (J/m^2)	1.78×10^{-2}	1.78×10^{-2}	1.78×10^{-2}
σ_e (J/m^2)	5.14×10^{-2}	8.25×10^{-2}	8.22×10^{-2}

It is assumed that $\gamma = l/l^*$, where l and l^* are the thickness of a mature crystallite and of the critical crystalline nucleus. T_m^0 can be determined from the crossing point of the $T_m = T_c$ line with the extrapolation of T_m as a function of T_c. This procedure is equivalent to an extrapolation to infinite lamellar thickness and the extrapolated equilibrium melting points are in the range of 282–292 °C and are also listed in Table 2. The T_m^0 determined from our experimental data is close to that reported in the literature by using the T_c ranged from 200 to 250 °C [43]. It can also be seen that the value of T_m^0 increases with the addition of 1 wt% layered silicate, suggesting that the crystalline phase in 1 wt% PLSNs is more perfect than that of pure PEN. By adding more layered silicate into PEN up to 3 wt%, the T_m^0 slightly decreases as the content of layered silicate increases. This phenomenon is probably due to the presence of more heterogeneous nucleation to reduce the perfection of PEN crystallite in PLSNs.

The regime theory of crystal growth is applied to analyze those crystal growth data to obtain thermodynamic parameters related to the crystallization process. It has to be emphasized that overall crystallization rate are not as simple to be interpreted as spherulitic radial growth because of the combination of nucleation and growth phenomena. According to the regime theory of crystal growth, the temperature dependence of the linear growth rate (G) is given as follows:

$$G = G_0 \exp\left[\frac{-U^*}{R(T_c - T_\infty)}\right] \exp\left[\frac{-K_g}{fT_c\Delta T}\right] \quad (6)$$

where G_0 a pre-exponential term; U^* the diffusional activation energy for the transport of crystallizable segments at the liquid–solid interface; T_∞ the hypothetical temperature below which viscous flow ceases; $f = 2T_c/(T_m^0 + T_c)$, a correction factor that accounts for the change of ΔH_f^0 (enthalpy of fusion of the perfect crystal) with the temperature. The nucleation constant K_g contains contributions from the surface free energies, and it can be obtained from Eq. (6):

$$K_g = \frac{4b\sigma\sigma_e T_m^0}{\beta k \Delta H_f^0} \quad (7)$$

where b is the distance between two adjacent fold planes; σ and σ_e are the lateral and folding surface free energy; k is the Boltzmann constant; and β is a parameter which depends on the regime of crystallization. The parameter β used in Eq. (7) is 1 in regimes I and III and 2 in regime II. Because the spherulite size of PLSNs is too small to estimate, the half time of crystallization $t_{1/2}$ instead of spherulitical growth rate G can be used. Therefore, Eq. (5) can be rewritten as follows:

$$\ln\left(\frac{1}{t_{1/2}}\right) + \frac{U^*}{R(T_c - T_\infty)} = \ln G_0 - \frac{K_g}{fT_c\Delta T} \quad (8)$$

Hoffman et al. [42] found $T_\infty = T_g - 30$ K and $U^* = 1500$ cal/mol by fitting the crystallization rate data for various polymers with Eq. (8).

Fig. 8 shows the plots of $\ln(1/t_{1/2}) + U^*/[R\,(T_c - T_\infty)]$ versus $1/[fT_c\Delta T]$ for PEN and PLSNs. The K_g values obtained from the slope of Fig. 6 are listed in Table 2. The data of b of β crystalline form is 1.56 nm according to the lattice parameter of PEN and the bulky enthalpy of fusion of perfect crystal ΔH_f^0 is 190 J/g [44,45]. In order to determine to which regime the data in the selected crystallization temperatures belong, the Lauritzen Z test is usually applied [46]. Z is a quantity defined by

$$Z \approx 10^3 \left(\frac{L}{2a_0}\right)^2 \exp\left(-\frac{X}{T_c\Delta T}\right) \quad (9)$$

where L is the effective lamellar width and a_0 is the width of the molecular chain in the crystal. According to this test, regime I crystallization kinetics are followed if the

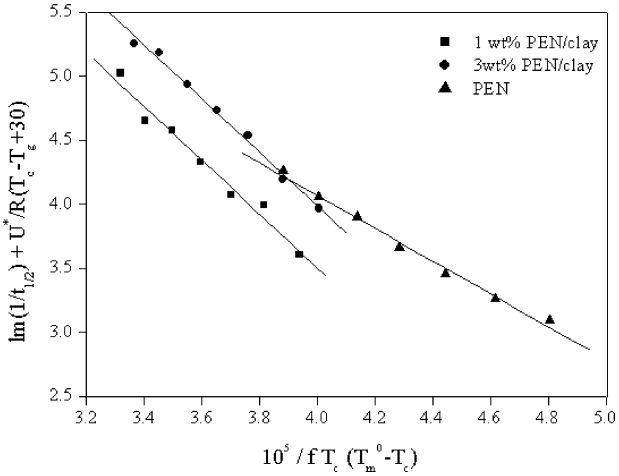

Fig. 8. Plots of $\ln(1/t_{1/2}) + U^*/[R\,(T_c - T_\infty)]$ versus $1/[fT_c\Delta T]\times10^5$ for PEN and PLSNs.

substitution of $X=K_g$ into the test results in $Z\leq 0.01$. If with $X=2K_g$ the test contains $Z\geq 1.0$, regime II kinetics are followed. As point out by Lauritzen and Hoffman [47], it is more convenient to the known value of K_g and the inequalities for Z to obtain the values of L in regimes I or II and to estimate if such values of L are realistic. The α crystalline unit cell of PEN is triclinic unit cell with the lattice parameter $a=6.51$ Å, $b=5.75$ Å, $c=13.2$ Å, $\alpha=81.33°$, $\beta=144°$, $\gamma=100°$, while the β crystalline unit cell is also triclinic with the lattice parameter $a=9.26$ Å, $b=15.59$ Å, $c=12.73$ Å, $\alpha=121.6°$, $\beta=95.57°$, $\gamma=122.52°$. It will be pointed out later (Fig. 8) the crystalline structure in the selected crystallization temperatures is β crystalline form. Therefore, the thickness of a monomolecular layer, b_0, is 0.57 nm and the chain width, a_0, is 0.65 nm [45]. Assuming $Z\leq 0.01$ and substituting $X=K_g$ into the Z-test, L will be smaller than 0.045 nm. This is clearly unrealistic. Assuming $Z\geq 1.0$ and substituting $X=2K_g$ into the Z-test, we obtain $L\geq 4.99$ nm and it is reasonable for PEN. Therefore, the crystallization regime is determined to be regime II.

Because the content of additional layered silicate is low, the parameter of b and ΔH_f^0 can be assumed to be the same as those of pure PEN. Therefore, the $\sigma\sigma_e$ data of the PEN and PLSNs are also determined from Eq. (7) and are in the range of 9.15×10^{-4}–14.68×10^{-4} J^2/m^4. For comparison, the $\sigma\sigma_e$ data of isotactic polystyrene (iPS) is 1.53×10^{-4} J^2/m^4 [48] and is much smaller than those of PEN and PLSNs. That is probably due to the presence of the bulky naphthalene ring to limit the chain flexibility and increase the end surface free energy σ_e leading to an increase in $\sigma\sigma_e$.

Fig. 9 shows X-ray diffraction data of PEN, 1 and 3 wt% PLSNs after melting at 300 °C and then quenching to the temperature in the range of 208–220 °C. X-ray data of PEN shows three intense reflections, (−1 −1 1), (0 2 0) and (2 −4 2), at $2\theta\cong 16.4$, 18.5 and 25.5° characteristic of the β crystalline form. The peak positions of these reflections of PLSNs are almost equivalent to those of PEN but the peak profiles of PLSNs are slightly broader than those of PEN matrix. These results indicate that the PEN and PLSNs have the same crystalline structure. Therefore, our previous assumption that PLSNs have the same b of β crystalline form as that of pure PEN matrix is reasonable.

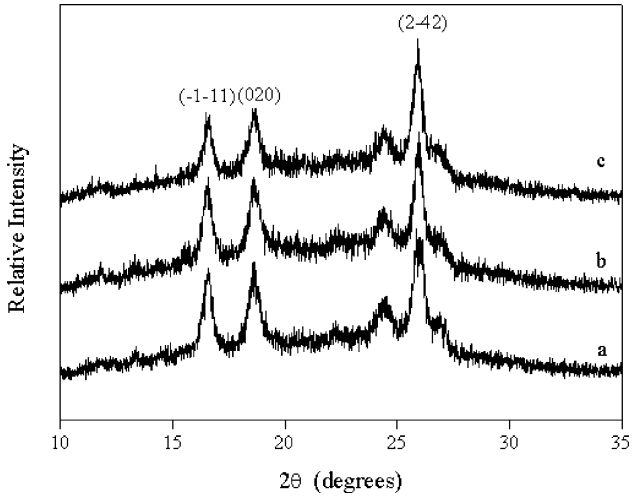

Fig. 9. X-ray diffraction scans of (a) PEN, (b) 1 wt % PLSNs and (c) 3 wt % PLSNs after melting at 300 °C and then quenching to various T_cs.

4. Conclusions

The PLSNs have been successfully prepared through the direct insertion of PEN polymer chains from the melt into the surface-treated clay and contained exfolicated silicate layers within a PEN matrix. Mechanical and barrier properties of the fabricated nanocomposites measured by dynamic mechanical analysis and permeability analysis show significant improvements in the storage modulus and water permeability when compared to neat PEN. The $\sigma\sigma_e$ data of the PEN and PLSNs are in the range of 9.15×10^{-4}–14.68–10^{-4} J^2/m^4, which is much higher than that of isotactic polystyrene (iPS). This is probably due to the presence of the bulky naphthalene ring to limit the chain flexibility and increase the end surface free energy σ_e leading to an increase in $\sigma\sigma_e$.

Acknowledgements

The financial support provided by NSC through the project NSC92-2622-E-005-006-CC3 was greatly appreciated.

References

[1] Giannelis EP. Adv Mater 1996;8:29.
[2] Okada A, Usuki A. Mater Sci Eng 1995;C3:109.
[3] Ogawa M, Kuroda K. Bull Chem Soc Jpn 1997;70:2593.
[4] Alexandre M, Dubois P. Mater Sci Eng 2000;28:1.
[5] Ray SS, Okamoto M. Prog Polym Sci 2003;28:1539.
[6] Lagaly G. Appl Clay Sci 1999;15:1.
[7] LeBaron PC, Wang Z, Pinnavaia TJ. Appl Clay Sci 1999;15:11.
[8] Liu L, Qi Z, Zhu XJ. Appl Polym Sci 1999;71:1133.
[9] Kim SH, Kang SW, Park JK, Park YH. J Appl Polym Sci 1998;70:1065.
[10] Nakamae K, Nishino T, Tada K, Kanamoto T, Ito M. Polymer 1993;34:3322.
[11] Mencik Z. Chem Prum 1967;17:78.
[12] Zachmann HG, Wiswe D, Gehrke R, Riekel C. Makromol Chem Suppl 1985;12:175.
[13] Buchner S, Wiswe D, Zachmann HG. Polymer 1989;30:480.
[14] Kim SJ, Nam JY, Lee YM, Im SS. Polymer 1999;40:5623.
[15] Cakmak M, Wang YD, Simhambhatla M. Polym Eng Sci 1990;30:721.
[16] Murakami S, Nishikawa Y, Tsuji M, Kawaguchi A, Kohjiya S, Cakmak M. Polymer 1995;36:291.
[17] Cakmak M, Lee SW. Polymer 1995;36:4039.
[18] Murakami S, Yamakawa M, Tsuji M, Kohjiya S. Polymer 1996;37:3945.
[19] Okamoto M, Kubo H, Kotaka T. Macromolecules 1998;31:4223.

[20] Nilno H, Yabe A, Nagano S, Miki T. Appl Phys Lett 1989;54:2159.
[21] Tsuji M, Fernando A, Novillo L, Fujita M, Murakami S, Kohjiya SJ. Mater Res 1999;14:251.
[22] Lee SW, Cakmak MJ. Macromol Sci Phys 1998;B37:501.
[23] Liu J, Sidoti G, Hommema JA, Geil PH, Kim JC, Cakmak MJ. Macromol Sci Phys 1998;B37:567.
[24] Maiti P, Okamoto M. Macromol Mater Eng 2003;288:440.
[25] Lincoln DM, Vaia RA, Krishnmoorti R. Macromolecules 2004;37: 4554.
[26] Lincoln DM, Vaia RA, Wang ZG, Hsiao BS. Polymer 2001;42:1621.
[27] Nam PH, Maiti P, Okamoto M, Kotaka T, Hasegawa N, Usuki A. Polymer 2001;42:9633.
[28] Maiti P, Nam PH, Okamoto M, Kotaka T, Hasegawa N, Usuki A. Macromolecules 2002;35:2042.
[29] Maiti P, Nam PH, Okamoto M, Kotaka T, Hasegawa N, Usuki A. Polym Eng Sci 2002;42:1864.
[30] Maio ED, Iannace S, Sorrentino L, Nicolais L. Polymer 2004;45: 8893.
[31] Hao J, Yuan M, Deng XJ. Appl Polym Sci 2002;86:676.
[32] Tseng CR, Wu JY, Lee HY, Chang FC. Polymer 2001;42:10063.
[33] Wu TM, Hsu SF, Wu JY. J Polym Sci Polym Phys 2002;40:736.
[34] Wu TM, Hsu SF, Chien CF, Wu JY. Polym Eng Sci 2004;44:2288.
[35] Wu TM, Wu JY. J Macromol Sci Phys 2002;B41:17.
[36] Wu TM, Hsu SF, Wu JY. J Polym Sci, Polym Phys 2002;40:736.
[37] Avrami MJ. Chem Phys 1939;7:1103.
[38] Avrami MJ. Chem Phys 1940;8:212.
[39] Wunderlich B. Macromolecular physics. vol. 3. New York: Academic Press; 1980.
[40] Alamo RG, Mandelkern L. Macromolecules 1991;24:6480.
[41] Hoffman JD, Weeks JJ. J Res Nat Bur Stand 1962;66A:13.
[42] Hoffman JD. Polymer 1983;24:3.
[43] Kim SK, Ahn SH, Hirai T. Polymer 2003;44:5625.
[44] Buchner S, Wiswe D, Zachmann HG. Polymer 1989;30:480.
[45] Lee WD, Yoo ES, Im SS. Polymer 2003;44:6617.
[46] Lauritzen JI. J Appl Phys 1973;44:4353.
[47] Lauritzen JI, Hoffman JD. J Appl Phys 1973;44:4340.
[48] Edwards BC, Phillips PJ. Polymer 1974;15:351.